applied sciences

MDPI

Article

High-Expansion Foam: A Risk Control Option to Increase Passenger Ship Safety during Flooding

Dracos Vassalos [1,*], Donald Paterson [1], Francesco Mauro [1], George Atzampos [2], Peter Assinder [3] and Adam Janicek [3]

[1] Maritime Safety Research Centre (MSRC), Department of Naval Architecture, Ocean and Marine Engineering, University of Strathclyde, Glasgow G4 0LZ, UK; d.paterson@strath.ac.uk (D.P.); francesco.mauro@strath.ac.uk (F.M.)
[2] Royal Caribbean Group, 20100 Turku, Finland; gatzampos@rccl.com
[3] Minova, Addlestone KT15 2NX, UK; peter.assinder@minovaglobal.com (P.A.); adam.janicek@minovaglobal.com (A.J.)
* Correspondence: d.vassalos@strath.ac.uk

Featured Application: The present study highlights the possible benefits for passenger ship safety by installing passive and active risk control options realised with high-expansion foam. The application of foams with proper permeability characteristics may improve the survivability of a passenger ship after an accident, as highlighted in the provided test cases performed with standard and advanced damage stability calculations.

Abstract: In naval architecture, the standard way adopted to reduce the risk of potential loss of life for passenger ships after an accident is via regulations. In case of flooding, this explicitly implies the introduction of fixed watertight bulkheads, permanently modifying the internal ship's layout. Damage stability regulations constantly aim at higher safety standards; therefore, the layout reconfiguration of an existing vessel may be essential to meet new requirements, leading to higher costs for retrofitting. Furthermore, increasing fragmentation of the internal layout has a physical limit, neglecting the possibility to elevate standards above a particular upper limit. In this view, innovative solutions give the chance to exceed such a limit. The present work describes the advantages of high-expansion foam application for passive and active protection from flooding events. The possibility to have a material granting sufficient water tightness allows installing fixed or deployable barriers that increase the safety level of the ship. Here, besides the description of the foam characteristics, the application on a reference passenger ship highlights the advantages of passive and active foam barriers to limit flooding and drastically reduce the risk of loss of lives. The changes in the limiting stability margins required by regulations and the analysis of dynamic flooding simulations for specific damage cases demonstrate the benefits of foam installation onboard passenger ships as a risk control option.

Keywords: ship safety; damage stability; risk control; high-expansion foam

Citation: Vassalos, D.; Paterson, D.; Mauro, F.; Atzampos, G.; Assinder, P.; Janicek, A. High-Expansion Foam: A Risk Control Option to Increase Passenger Ship Safety during Flooding. *Appl. Sci.* **2022**, *12*, 4949. https://doi.org/10.3390/app12104949

Academic Editor: Koji Murai

Received: 28 March 2022
Accepted: 12 May 2022
Published: 13 May 2022

1. Introduction

Survivability of passenger ships after an accident is a parameter that needs to be assessed during the ship design process to evaluate the potential risk of loss of life associated with the accident itself [1–3]. This has become (and will always be) even more relevant due to the incremental growth of passengers in new cruise ship designs [4]. According to the statistics of casualties involving cargo and passenger ships in the last 10 years [4], the following ranking can be provided: 27% loss of control, 26% collisions, 15% contacts, 13% groundings/stranding, 12% damage, 5% fire, 1% flooding, and 1% capsize. The majority of the casualties are related to collisions and groundings/contacts, which are damage types that intrinsically implicate flooding and the potential sinking or capsizing

of the vessel [5]. To this end, regulations impose restricting requirements for the damage stability of passenger ships [6,7]. The normative request of incrementally higher standards for damage stability impacts the internal layout of a new passenger ship design [8]. The standard answer of naval architects concerning the request of increasing survivability after an accident corresponds to an increased subdivision of internal spaces [9–11]. However, reacting to more restrictive safety requirements through a fractal fragmentation of the internal ship volume also has a physical limit for new designs [12], decreasing the ship earning potential (more weight and less usable space) without further increasing its safety. Moreover, a substantial reconfiguration of internal spaces may be technically impossible or too expensive for the refitting of existing ships for fulfilling new safety requirements [13].

An efficient and cost-effective way to boost the safety of passenger ships should aim at overtaking the actual plateau of the safety level reached by modern designs, looking more into residual risk mitigation rather than total risk prevention. Mitigation of the residual risk implies the adoption of technological innovation where solutions are likely to be found in the shorter-term and, more than likely, be cost-effective. On the other hand, for the specific cases of damage stability, residual risk mitigation requires a thorough understanding of the loss modalities of a ship due to flooding, thus the availability of appropriate methods, tools, and techniques capable of meaningfully addressing the physical phenomena involved in the flooding process [14,15]. In this sense, the application of risk mitigation systems based on detailed analyses of the flooding process designed jointly with the application of materials granting sufficient water tightness and mechanical properties could drastically increase the safety level of a passenger ship after a flooding accident [16,17].

An effective result of this radical change in the approach to flooding risk management for passenger ships is provided by the AREST (Adaptive REconfigurable Safety Technology) systems, related to a University of Strathclyde Patent (patent no. PCT/GB 2017/050681), combining accurate flooding vulnerability analysis with the use of high-expansion foams to restore or limit the loss of buoyancy due to flooding. Such a system is composed of passive solutions, active solutions, or a combination of both of them. Traditionally, mitigation measures address only one of the following options for risk reduction: limiting flooding occurrence, increasing the residual stability or limiting/preventing flooding progression. Ship reinforcement [18] is a design measure that aims at reducing the potential dimension of a breach, thus limiting the flooding occurrence. Permeability reduction aims at increasing vessel residual stability by using different strategies, such as counter ballasting, application of foams, systems employing C02-based fire systems to activate air-bags inside damaged compartments, etc. [19]. The fragmentation of flooding progression is achieved by increasing the number of watertight doors [20] or changing the internal layout of the ship [21]. The AREST system could in principle address all the above-mentioned options.

In the present work, after an introduction to the methods adopted for the damage stability assessment of a passenger ship and the description of passive and active AREST systems, the main characteristics of the high-expansion foam will be described, highlighting its suitability for deployment as flooding countermeasures. The adoption of such countermeasures will be demonstrated on a reference large cruise ship, showing the global safety increase granted by the adoption of passive systems, together with the advantages provided by active countermeasures in specific critical flooding scenarios.

2. Damage Stability Assessment of a Passenger Ship

One of the essential issues necessary to identify the mitigation measures for the residual risk of ship loss due to flooding is the evaluation of the survivability of the ship after an accident. The behaviour of a damaged ship after an accident is for sure a relevant attribute for passenger ship design, requiring the adoption of time domain tools capable to handle vessel dynamics coupled with flooding of water [22,23]. However, it is a common designer practice to treat this issue with a simplified regulation-compliant approach based on static calculations only [6,7].

In any case, the framework for the determination of passenger ships' survivability after flooding necessitates the definition of breaches dimensions and locations for different kinds of damage types. To this end, two different paths may be pursued to identify distributions of damage characteristics, depending on the desired level of accuracy and the availability of adequate tools and datasets, namely:

1. *Probabilistic method*: the distributions for damage characteristics are derived from statistics of accidents, dividing the damages between collisions [24], side groundings [25] and bottom groundings [26].
2. *Direct method*: damage characteristics distributions derive from scenario-based simulations, implying the hindcast analysis of traffic routes in a given area [27,28] and the execution of crash analyses to determine the damage dimensions [29].

Regardless of the selection of one of the two methods to derive the damage characteristics distributions, it is necessary to determine the relevant cases needed to assess ships' survivability. The measure of survivability is given by an index A defined as follows by the actual regulatory framework [7]:

$$A = \sum_{k=1}^{3} \sum_{j=1}^{3} w_{jk} A_{jk} \tag{1}$$

where k indicates the damage type (collision, side, and bottom groundings), j indicates the calculation draught (light service, partial or deepest subdivision droughts), w_{jk} are the weights between the calculation conditions [30], and A_{jk} are the partial indices evaluated on specific combinations of damage types and draughts. The partial A_{jk} indices of Equation (1) have the following formulation:

$$A_{jk} = \sum_{i=1}^{N_c} p_{ijk} s_{ijk} \tag{2}$$

where i distinguishes each of the N_c groups of compartments identifying a unique damage case. The so-called p-factors p_{ijk} are associated with the occurrence of the specific damage case [31] and the s-factors s_{ijking} are linked to the probability to survive at the damage. Traditional methods derive p-factors from analytical integration for collision damages only [32]. Modern methodologies prefer the adoption of a more flexible non-zonal approach [26], covering collisions and bottom/side groundings, evaluating A_{jk} with a randomised quasi-Monte Carlo process [33].

The evaluation of p-factors is directly associated with the sampling process of damage distribution characteristics [31,33], thus adopting a probabilistic or a direct approach for the damage distribution is changing the final p-values but not the calculation process itself. On the contrary, the determination of s-factors is strongly influenced by the method adopted to perform damage stability calculation; i.e., through a static or a dynamic assessment.

2.1. Static Assessment

The assessment of s-factor through static calculations is based on empirical formulations derived from the static residual GZ curve for all the intermediate and final stages of flooding associated with a damage case. According to SOLAS [7], the s_{ijk} contributing to A_{jk} calculation should be determined from:

$$s_{ijk} = \min_{1<h<N_{stage}} \left(s_{int_{ijkh}}, s_{final_{ijk}} s_{M_{ijk}} \right) \tag{3}$$

where s_{int} are the survivability factors for all the N_{stage} intermediate flooding stages until the final equilibrium stage, s_{final} is the survivability in the final equilibrium stage, and s_M is the survivability to external heeling moments in the final equilibrium stage. These quantities can be calculated as follows for passenger ships:

$$s_{int_{ijkh}} = \begin{cases} 0 & \text{if } \varphi_e > 15^\circ \\ \left(\frac{\min(GZ_{max}, 0.05)}{0.05} \frac{\min(Range, 7)}{7}\right)^{\frac{1}{4}} & \text{if } \varphi_e \leq 15^\circ \end{cases} \quad (4)$$

$$s_{final_{ijk}} = K\left(\frac{\min(GZ_{max}, TGZ_{max})}{TGZ_{max}} \frac{\min(Range, TRange)}{TRange}\right)^{\frac{1}{4}} \text{ with } \begin{cases} K = 1 & \text{if } \varphi_e \leq 7^\circ \\ K = 0 & \text{if } \varphi_e \geq 15^\circ \\ K = \sqrt{\frac{15-\varphi_e}{8}} & \text{otherwise} \end{cases} \quad (5)$$

$$s_{Mijk} = \min\left(\frac{(GZ_{max} - 0.04)\Delta}{M_{heel}}, 1\right) \quad (6)$$

where GZ_{max} is the maximum of the residual righting lever curve for each damage case and loading condition. GZ_{max} must fall within the positive interval *Range* between the equilibrium angle φ_e and φ_v, the minimum between the capsize and the unprotected opening immersion angle. *TRange* and TGZ_{max} assume different values for cases involving flooding of car deck in Ro-pax ships (0.20 m for TGZ_{max}, 20° for *TRange*) and not (0.12 m for TGZ_{max}, 16° for *TRange*). Δ is the ship displacement and M_{heel} is the external moment, which is the maximum between moments due to wind, movement of passengers and launch of survival crafts. The s-factor formulations in Equations (4)–(6) are all with values in [0, 1], thus the s-factors represent a probability to survive a specific event in a specific flooding condition. Figure 1 shows an example of a residual GZ curve with the associated parameters relevant for stability assessment.

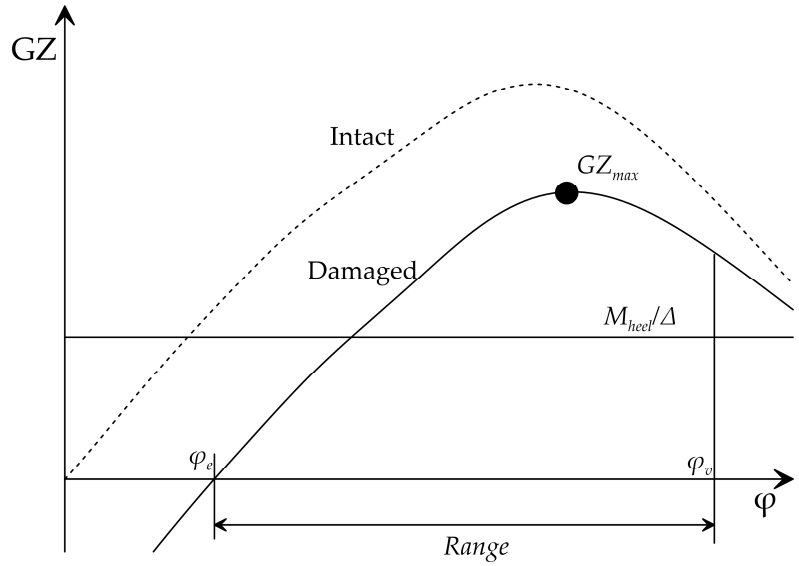

Figure 1. Residual GZ curve for static damage stability calculations.

From these calculations, three case categories can be identified, according to the s-factor value:

1. $s_{ijk} = 0$: cases where the vessel can be considered statically capsized or with insufficient residual stability margin.
2. $0 < s_{ijk} < 1$: cases where there could be a reduced reserve of stability that may lead to capsizing in case a wave environment is faced.
3. $s_{ijk} = 1$: cases where the vessel can be considered safe and potentially have a sufficient reserve of stability to face waves.

The resulting *s* values combined with the associated *p* lead to the determination of the attained survivability index *A*, which is expected to be compared with the required subdivision index *R* defined by SOLAS [7], ensuring that $A_{jk} \geq 0.9R$. *A* index is not the only metric suitable to measure survivability, and alternative parameters can be preferred,

as probability of loss of lives (PLL) and GM margin. From an operator's perspective, the former is the most important and familiar measurement with direct impact on the operability of their vessels. However, from a static assessment, other information can be derived, concerning the vulnerability of the ship. Such indications are relevant to identifying critical zones, requiring attention by the designer.

Static Risk Profile

The static survivability assessment is performed on the damage cases derived from the sampling of marginal distributions, grouped in unique damage scenarios with associated p-factors, and determining the associated survivability through Equations (4)–(6). As already mentioned, each damage case has an occurrence p_{ijk} and a probability to survive that damage case defined by s_{ijk}. These two factors can be representative of risk. The factor p_{ijk} $(1 - s_{ijk})$ can be used to give a rough estimate of the capsize risk associated with a particular damage case. Figure 2 gives an example for two different passenger ships (one cruise ship and one Ro-pax), considering the collision damage cases resulting from three repetitions of 10^5 breaches. The Figure shows the damages as they are located along the ship length, reporting the non-dimensional location of the damage centre X_D/L_s. The diagram highlights the areas having higher risk of capsize due to flooding, thus the area where designers should focus to improve ship safety. The static risk profile gives useful information to compare potential risk of different ships or design solutions; however, it is not enough to have an effective and realistic vision of the flooding process in the most critical cases.

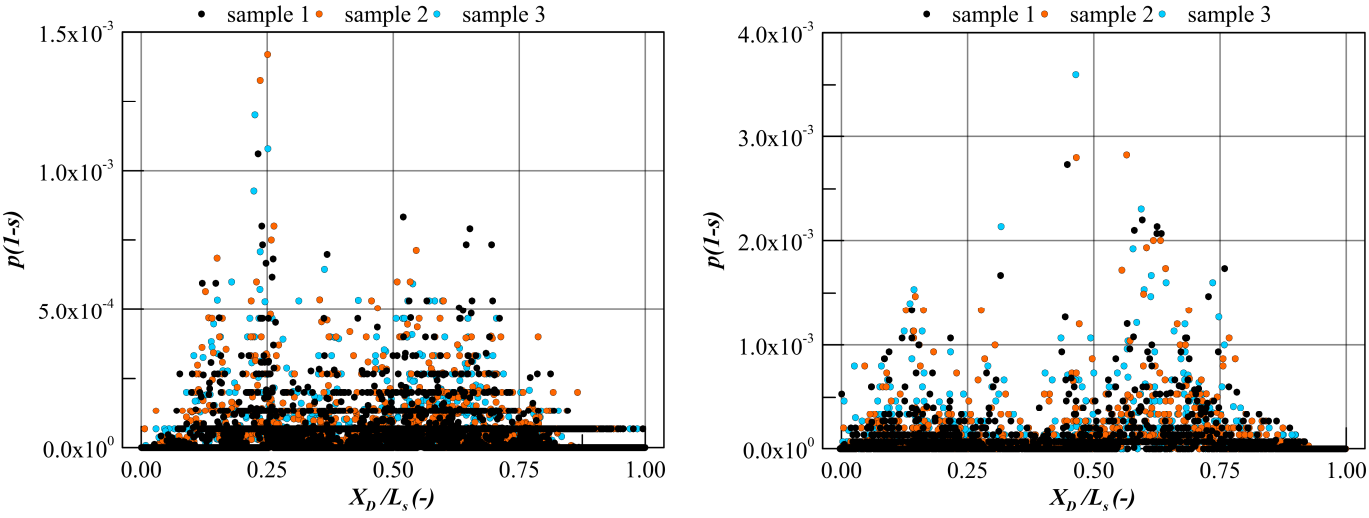

Figure 2. Static risk profile for a cruise ship (**left**) and a Ro-pax (**right**).

2.2. Dynamic Assessment

Static assessment is a simplified approach dealing with calm water cases only; however, a detailed knowledge of the possible risk of capsize due to flooding needs to consider a direct evaluation of the flooding process, including adverse sea conditions. The assessment of damage stability with direct calculations requires the modelling of complicated phenomena, related to the coupling between ship motions and the dynamic process of floodwater and its interaction with the ship and the wave environment. The modelling can be performed with different simplification levels, leading to different confidence for the obtained results.

A good compromise between accuracy and calculation effort is reached by the adoption of time domain simulations based on rigid body dynamics. Equations describing damaged ship behaviour are derived from fundamental motion principles: the law of conservation of linear and angular momentum. This law, normally applied to rigid bodies, is also extended to the internal fluid mass, resolved in a body-fixed system of reference. This leads to the

definition of six scalar equations for linear and angular motions. As an example, the three equations of angular motions have the following vector form:

$$\begin{aligned}(I'_s + I'_w)\cdot\tfrac{\mathrm{d}}{\mathrm{d}t}\vec{\omega'} + M_w\cdot\left[\vec{r'}_w \times \tfrac{\mathrm{d}}{\mathrm{d}t}\vec{v'}_{Gs}\right] + M_w\cdot\left[\left(\vec{\omega'}\times\vec{r'}_w\right)\times\vec{v'}_w\right] + \\ +M_w\cdot\left[\vec{r'}_w\times\left[\tfrac{d}{dt}\vec{v'}_w + \vec{\omega'}\times\left(\vec{v'}_{Gs}+\vec{v'}_w\right)\right]\right] + \\ +\tfrac{\mathrm{d}}{\mathrm{d}t}M_w\cdot\left[\vec{r'}_w\times\left(\vec{v'}_{Gs}+\vec{v'}_w\right)\right] + \left(\tfrac{d}{dt}I'_w\right)\cdot\vec{\omega'} + \vec{\omega'}\times\left[(I'_s+I'_w)\cdot\vec{\omega'}\right] = \vec{M'}_{Gs}\end{aligned} \tag{7}$$

where I_s and I_w are the ship and internal fluid mass moments of inertia; ω is the rotational velocity vector, M_w is the internal fluid mass and r_w and v_w are the position and velocity vectors of the internal fluid mass centre. v_{Gs} is the ship velocity vectors and M_{Gs} are the external moments acting on the ship. A more detailed explanation of all relevant terms and of the complete model in six degrees of freedom is given in [34]. The right-hand side of Equation (7) and the respective force vector of the rectilinear motions represent the external forces and moment acting on the vessel with respect of its centre of mass. The sloshing motions of the floodwater can be modelled as a lumped mass [35], while water ingress, the flooding progression and accumulation follow a simplified model based on Bernoulli equation. All these methods are implemented in software PROTEUS3, used for this study, which was tested and validated at the University of Strathclyde against numerous model experiments and benchmark tests on various vessel types [34].

As mentioned, time domain simulations imply the modelling of the water ingress-regress from the breach. Therefore, breach dimensions influence the flow rate entering/leaving the ship. For such a reason, different breaches leading to the same set of damaged compartments lead to different flooding simulations. This imply avoiding the grouping process performed in the static assessment to determine the p-factors. Thus, for a full dynamic assessment, the number of breaches N_b corresponds to the number of cases N_c. Consequently, the "dynamic p-factor" is a constant equal to $1/N_b$ and Equation (2) for a fully dynamic assessment becomes:

$$A_{jk} = \frac{1}{N_b}\sum_{i=1}^{N_b} s_{ijk} \tag{8}$$

Even though the nature of dynamic p-factor is different from the static case, the sampling process of damage characteristics remains the same, with the addition of the environmental characteristics. In fact, dealing with simulations in worldwide open sea conditions, a significant wave height H_s should be sampled for all breaches from a dedicated marginal distribution [36]. Such H_s is used to model an irregular sea state by means of a wave spectrum (usually Pierson Moskowitz or JONSWAP type). Here, dealing with time domain simulations, it is necessary to take into account the stochastic nature of an irregular sea environment. It is then necessary to perform multiple repetitions N_r of the same sea state (see Figure 3). Therefore, the survivability factor should not be determined as the survivability of a single simulation, but as the average of multiple realisation N_r with the same sea state, resulting in:

$$s_{ijk} = \frac{1}{N_r}\sum_{h=1}^{N_r} I_h \quad \text{where} \begin{cases} I_h = 1 & \text{if the ship survived} \\ I_h = 0 & \text{if the ship capsized} \end{cases} \tag{9}$$

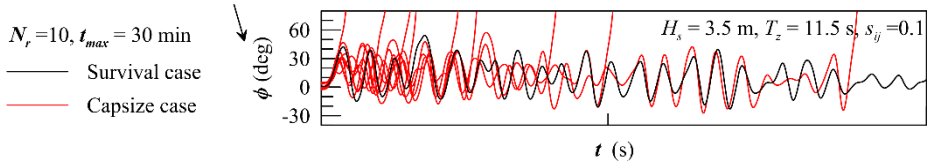

Figure 3. Example of ten realisations of the same damage in irregular waves for a cruise ship.

The function I in Equation (9) is not only influenced by the number of repetitions of each dynamic simulation, but also by the exposure time in the wave environment; thus, by the maximum simulation time t_{max} used for the simulations. Here, simulations were carried out setting t_{max} to 30 min as it is usual for probabilistic assessment of passenger ship survivability. However, not all capsize cases have the same nature and this should be investigated in detail.

Ship Loss Modalities

The identification of a capsize event and the evaluation of the time prior to this event after a damage is of utmost importance for the evacuation analysis of a vessel. In fact, in case a damage could potentially lead to the sinking of the vessel, it should be possible to evacuate passengers and crew in less than half an hour. However, capsizing may have different nature depending on the interaction between floodwater and vessel motions and this is usually identified with the flooding state they relate to. When the flooding process is studied, the following states can be identified after an accident:

1. *Transient*: is the first part of the flooding process. The water rapidly inrushes trough the breach, causing a rapid and large inclination into or away from the breach side. The oscillation occurs in a time interval generally shorter than the vessel natural roll period.
2. *Progressive*: in this stage, the water propagates though unprotected flooding paths within the ship, slowly diminishing stability until the vessel sinks, capsizes or reaches a stationary condition. This phase may take from minutes to hours.
3. *Stationary*: in this phase, there is no more significant water ingress/egress and the average ship motions are almost constant or with amplitude oscillation due to external loads only.

In case the capsize occurs during the transient phase, the consequences, in terms of loss of lives, are extreme, the phenomenon being too fast to start the evacuation process. When an accident occurs in calm water, then the detection of a capsize is only governed by floodwater progression. In all cases, it is possible to determine the time to capsize (TTC), which is an important parameter to establish the safety level of a vessel with dynamic simulations. The identification of loss modalities for a ship allows determining which are the damage cases that need more attention for the implementation of risk control options.

3. Solutions for Damage Stability Protection Using Foam: AREST System

As highlighted in the previous sections, the safety of a passenger ship after flooding is related not only to its hull shape, but also (and probably even stronger) to its internal layout. However, the internal layout of a passenger ship needs to address specific necessities for passenger leisure, together with safety requirements concerning other sources of risk of loss of lives, such as fire. Adding further constraints to the internal layout to mitigate flooding could compromise the earning potential of the ship. Therefore, it is necessary to look at possible solutions aimed to increase safety during a possible accident during the ship operation, thus increasing ship resilience to a failure event. The AREST system developed at the University of Strathclyde in collaboration with foam company MINOVA and design office Sea Transport Solutions is a step in this direction, with a set of available solutions cost-effectively reducing flooding risk. As a suitable risk control option against flooding should address critical cases leading to capsize during the transient and the progressive flooding stages, suitable solutions have to be found against both possibilities. Here, the focus is on

two protection systems specifically addressing the transient and progressive flooding case, using high expansion foam with adequate permeability and adhesion characteristics, fit for the whole life-cycle of any vessel. High expansion foam is not the only suitable option for a permanent foam installation, where other materials, such as polyurethane or fibre glass, in the form of foam core composite sandwich panel or foam-filled lattice composite panel, can be employed. However, having a single material for all of the possible AREST system is an advantage if the material has the required mechanical characteristics.

3.1. Permanent Foam Installation: AREST P1

This is a passive flooding protection system involving the installation of permanent foam in void spaces to provide additional reserve buoyancy when these spaces are directly damaged or indirectly flooded following an incident, thus increasing the ship's initial stability and restoration forces. Such installations act similar to buoyancy tanks, with the added benefit of being impermeable, thus providing buoyancy within the immediate damaged area. This kind of improvement in initial stability and additional reserve of stability aims at reducing the risk of transient capsize cases, which are also directly associated to an inadequate initial reserve of stability during the initial stages of flooding. To be effective upon installation, the foam should adhere to the vessel steel structure, prohibiting build-up of moisture between the foam and ship structure whilst offering effective insulation. Moreover, in any foam installation, particularly near passenger spaces, appropriate fire protection measures need to be ascertained to contain and control any potential fire risk that may ensue from the foam itself. This is an essential part of the derricking his novel technology, as part of the approval process by class and administration. Figure 4 shows a possible site for foam application in available void spaces on the lower decks of a passenger ship. With AREST P1 acting directly on the instantaneous initial stability and on the stability reserve, this system is appropriate to reduce risk of transient capsize in critical damage cases. On the other hand, this system is not designed to arrest flooding progression along the ship internal layout. Therefore, an alternative/complementary solution is necessary to limit progressive flooding.

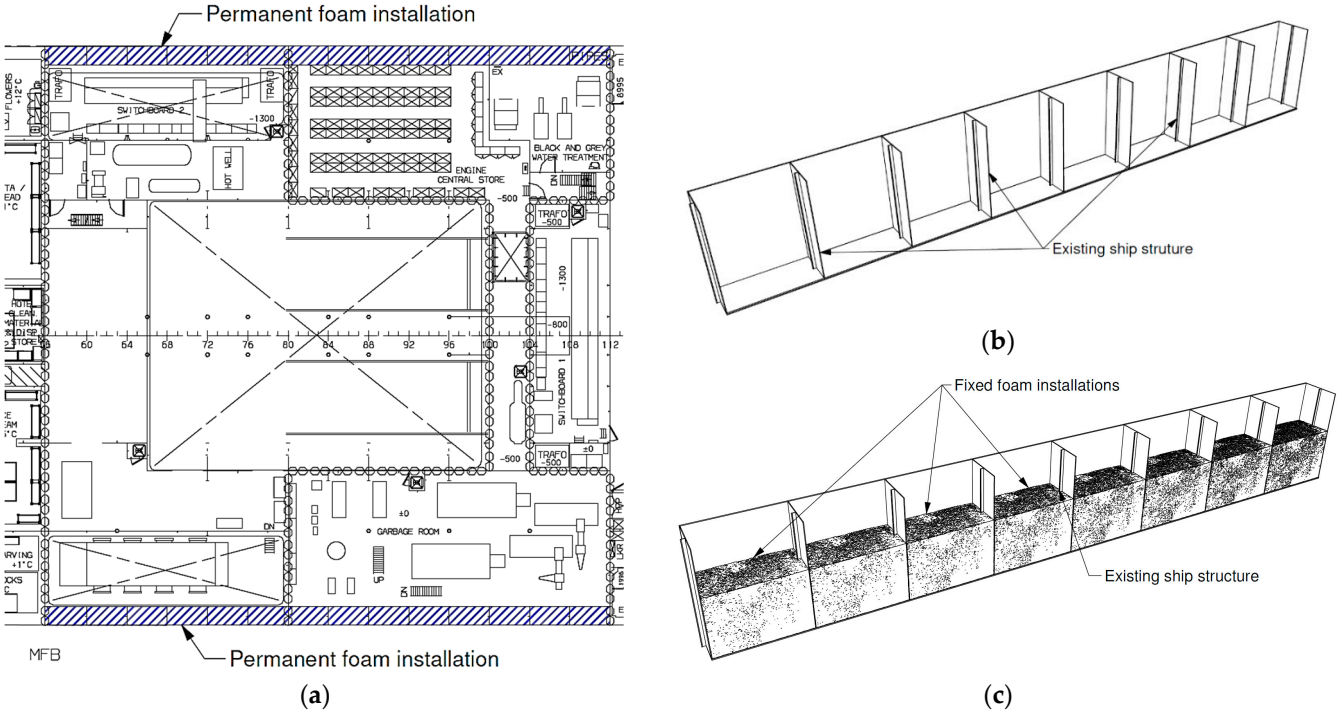

Figure 4. AREST P1 system; (**a**) permanent foam installation sites (blue) in a double hull. (**b**) Existing ship structures in the installation site. (**c**) Void spaces filled with foam.

3.2. Deployable Watertight Barriers: AREST A2

During the flooding process of a complex environment, the internal geometry of a ship and the progressive flooding paths can be divided in major progressive floodwater paths. Minor paths represent small corridors and spaces connected within each other in a specific zone, thus pathways that allow local flooding of the ship. Main paths are mainly large corridors connecting two contiguous zones of the ship, thus arteries that may rapidly spread floodwater along the ship (see Figure 5a). In order to most effectively deal with progressive flooding in ships, it is best to focus on blocking the major arteries.

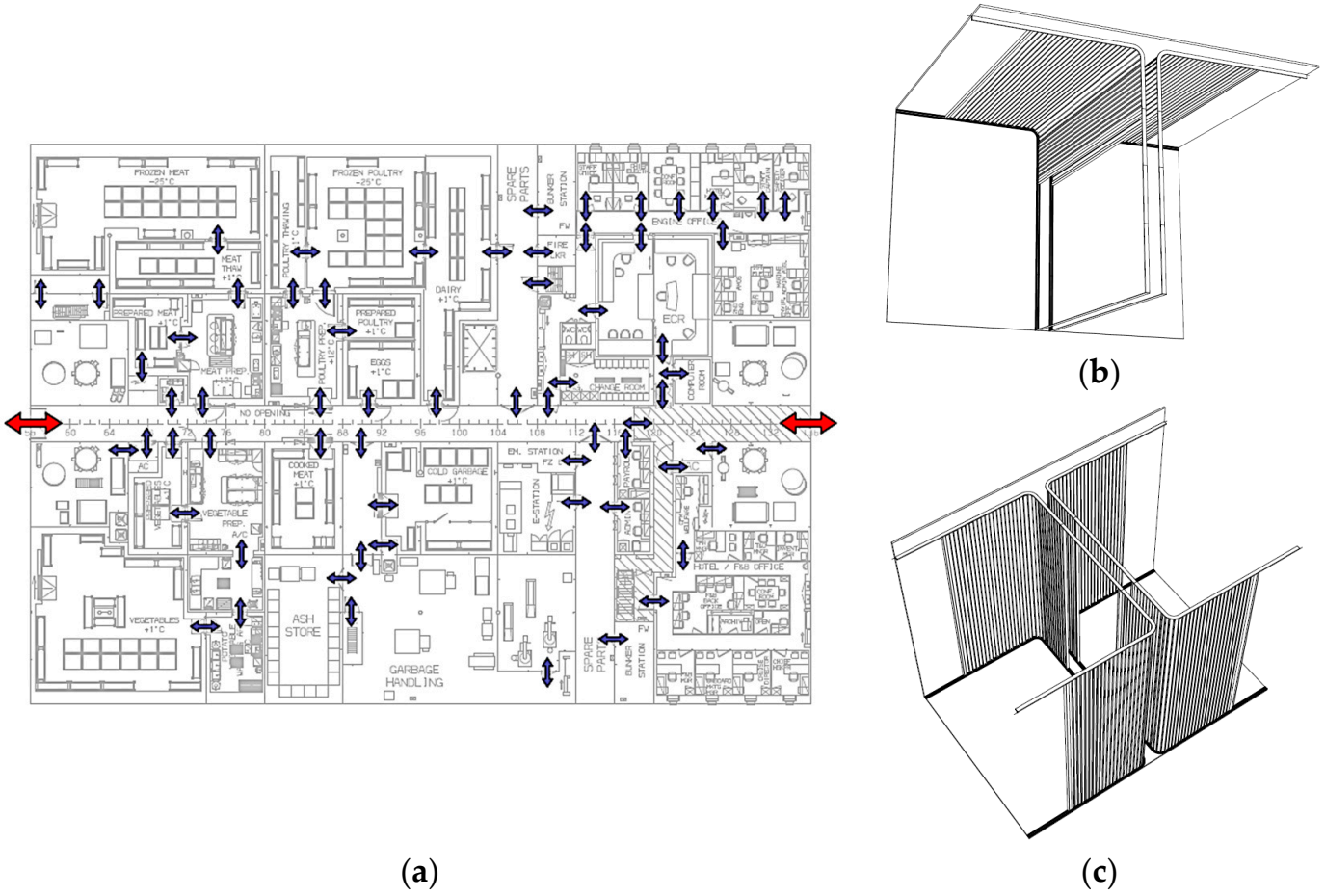

Figure 5. AREST A2 system; (**a**) main (red) and minor (blue) flooding path on a cruise ship deck zone. (**b**) Vertically deployable shutters. (**c**) Horizontally deployable shutters.

To this end, deployable barriers are a suitable solution that may contain flooding without modifying the internal layout of the vessel. AREST deployable barriers comprise two lightweight shutters made of GRP or steel laths (normally A-class fire-rated), distanced 30 cm apart. Shutters can be deployed also in case of fire casualties or drills. In case of flooding, the cavity between shutters is filled with expanding foam delivered from a compressed foam canister. The shutters are mechanically operated to be deployed vertically (see Figure 5b) or horizontally (see Figure 5c) to suit local structural details and arrangements. The barrier can also span distances up to 30 m, with intermediate supports and can be deployed within minutes to curtail and control previously identified critical floodwater pathways.

In this respect, from the results of time domain flooding simulations, an effective damage control plan could be set up and suitably executed with the aid, for example, of a suitable decision support system. This allows isolating the damage area following any foreseeable critical flooding event for which progressive flooding is responsible for loss.

Such an approach implies the execution of evacuation analyses for selected critical cases to identify that deployable barriers do not interfere with the evacuation process. This offers a distinct advantage over existing damage control plans, which rely entirely on fixed design measures, having limited flexibility and effectiveness with probable critical loss scenarios.

3.3. Foam Characteristics

The above-described passive and active solutions for marginal risk reduction imply the adoption of a material with specific characteristics. The adoption of foams in ship industry is usually focused on fire doors [37,38] or noise reduction [39]. Here the focus of the AREST system is primary on flooding; thus, additional characteristics for the foam are required. As development of the AREST systems were subjected to the process of novel technology qualification, as indicated earlier, a HAZID process was conducted, resulting in specific requests for the foam characteristics concerning permeability, adhesion, cohesion, compression, degradation over the ship life-cycle and, most importantly, protection against fire hazards from external sources and the foam itself.

3.3.1. Permeability

In order to determine the permeability of foam utilised within the previously described risk control options, it was deemed necessary to conduct a water absorption test on the proposed foam technology. By doing so, the mass of water absorbed by the foam can be quantified as a function of time and varying external water pressure. From these results, a determination can be made regarding an appropriate foam permeability value, with due consideration given to the anticipated exposure time of the foam to water and the pressures under which this might occur. To this end, two water absorption tests were conducted, the first under atmospheric pressure conditions and the second with incremental overpressure.

The first water absorption test was conducted at atmospheric pressure, with a foam specimen of 100 × 200 × 300 mm anchored fully immersed in water for a period of 28 days. The specimen was removed from the water and weighed at several intermediate stages to compare the wetted mass with its dry weight, thus determining the water absorbed as a function of the time exposure. Table 1 reports the results of the test at atmospheric pressure, highlighting that the foam water absorption ranges from 2% in weight after one day up to 2.7% after 28 days of exposure. From the observed data, it is evident that the rate of water absorption decreases with time, reaching an asymptotic value around about 3% conditioned on 28 days of exposure at atmospheric pressure.

Table 1. Foam water absorption as a function of time at atmospheric pressure.

Exposure Time (Days)	Water Absorption (%)
1	2.1
2	2.1
3	2.2
14	2.5
28	2.7

Having to deal with flooding of internal spaces of a ship, it is also necessary to check the behaviour of permeability with pressure values greater than atmospheric by means of an additional water absorption test, varying the level of overpressure on a fixed time interval. For this test, a cubic foam specimen of 100 × 100 × 100 mm was used. Foam sample specimens were fully immersed in water within a pressure vessel, see Figure 6. Compressed air was then injected into the vessel in a controlled manner, generating water overpressures acting on the foam of 0.5, 1, and 1.5 bars, with watertight integrity typically rated up to 1.5 bar (15 m water head). The test was carried out for a time interval of 3 h, being an appropriate time scale compliant with Safe Return to Port regulations. Table 2 reports the results, where an increase in foam permeability can be observed at water

pressures ranging up to 0.5 bar, moving from 1% to 2% permeability. Interestingly, at pressures beyond this point, it was found that the foam permeability was insensitive to increasing pressure, remaining at a constant value of approximately 2%.

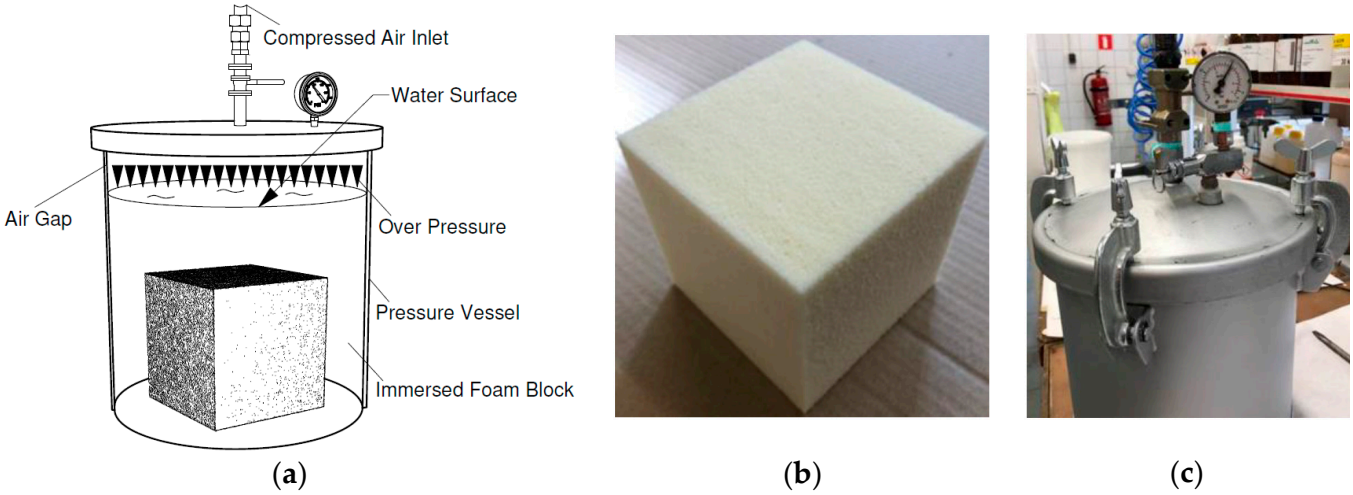

Figure 6. Overpressure water absorption test. (**a**) Test settings, (**b**) foam specimen, (**c**) pressure vessel.

Table 2. Foam water absorption as a function of overpressure during 3 h of exposure.

Overpressure (Bar)	Water Absorption (%)
0.0	1.0
0.5	2.0
1.0	2.0
1.5	2.0

With respect to the above-mentioned results outlined within the foregoing, it is important to consider the effects of scale and their impact on the permeability value calculated. The sample sizes used within the experiments are of the order of 0.001 m^3 in comparison to the static foam installations, which are of the order of 200–300 m^3 in size. This is important, as the manner in which the foam absorbs water is such that smaller sample sizes will demonstrate higher permeability than large ones. Consequently, the experiments are inherently conservative due to the scale at which they are conducted. This means that the wetted volume of foam relative to the specimen size will decrease with increasing foam volume.

This effect is further described in Figure 7, where an example of the general relationship between the sample size and the value of permeability determined is illustrated. Furthermore, the experiments conducted have assumed the entirety of the foam surface area to be in contact with water, thus increasing water uptake. However, in practice, it is more than likely that only a portion of the foam surface will be in contact with water and, thus, the water absorption in reality will be much less. For such reasons, it can be assumed that a permeability of the foam of 5% can be used for calculation purposes, allowing for a 3% safety margin on the experimental value.

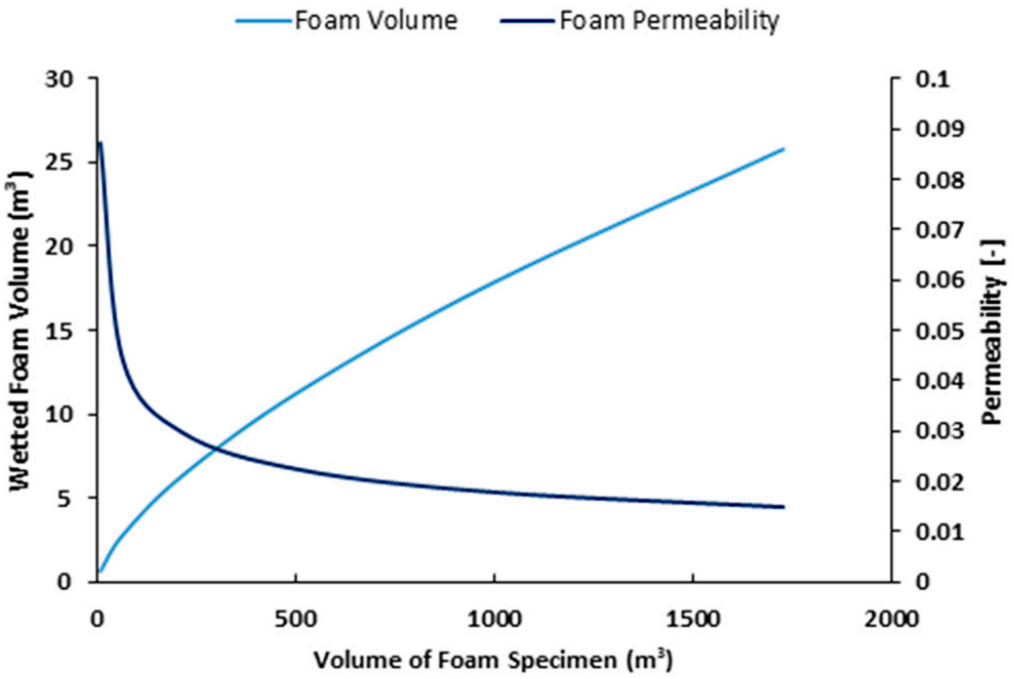

Figure 7. Effect of specimen size on permeability determination.

3.3.2. Adhesion and Cohesion

From the HAZID process the following adhesion and cohesion requirements were identified for the AREST risk control options:

- *AREST P1*: installations must remain in place during their service life and following a flooding incident, where they must withstand buoyant forces. Foam must possess sufficient cohesion to ensure the installation does not break apart when acted upon by buoyant forces.
- *AREST A2*: foam must have sufficient adhesion in order to create a watertight seal within the shutter arrangement. No critical cohesion requirements were identified.

Given the above, we determined the adhesive and cohesive properties of the foam by conducting a "pull-off" test. This works by measuring the force required in order to separate the foam from a given bonded surface (adhesion) or alternatively the force necessary to separate the foam body itself (cohesion).

Adhesion is a property that varies depending on the nature of the bonding surface and increases when moving from smoother to coarser surfaces. However, in this case steel was considered appropriate given that the targeted spaces for such installations (voids) have predominantly steel surfaces. The pull-off test, also referred to as a stud-pull test, works by firstly applying a layer of foam to a steel plate and allowing it to cure. Following this process, an adhesive connection is made between a metal stud and the foam surface, using an epoxy resin of a stronger bond than that expected by foam adhesion. An incision is then made in the foam around the perimeter of the stud, such that foam adhesion to the plate is the only force resisting separation. An apparatus is then used in order to pull the stud/foam assembly from the steel plate and the force required to do so is recorded, thus providing a measure of foam adhesion. Figure 8 reports the pull test diagram and the different phases of the test.

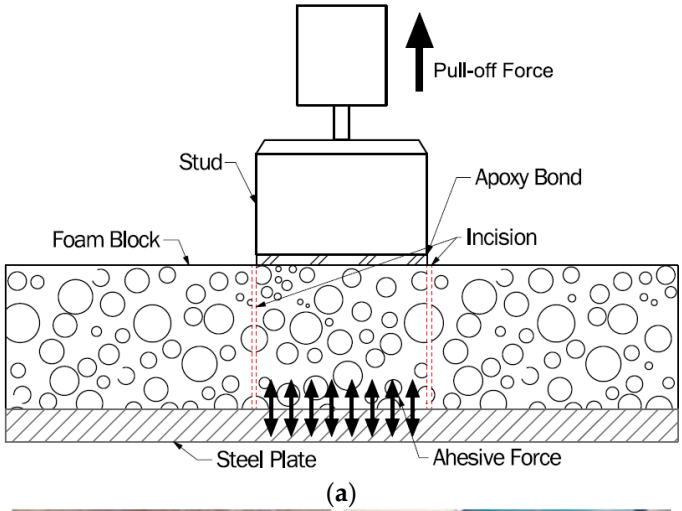

(**a**)

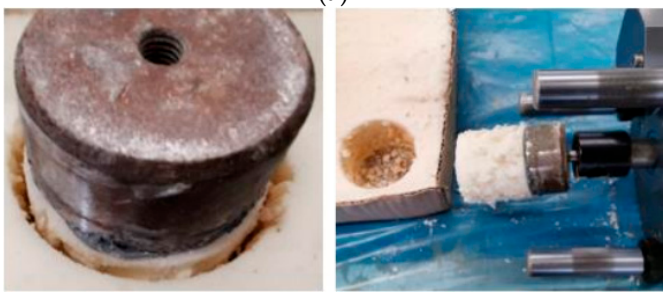

(**b**)

Figure 8. Pull off test; (**a**) test diagram. (**b**) Stud fixed to foam/plate assembly (**left**); foam separated from steel plate (**right**).

The foam cohesive properties were also measured in a similar way (same process, without the steel plate). From the test result, the foam has an adhesion to steel of 0.13 MPa and a cohesion at the foam surface of 0.19 MPa. As a result, and given the contact area of the foam installation to the surrounding ship structure, it is highly unlikely that the foam body would break free from its bonds even when fully immersed.

3.3.3. Compressibility

The last critical system property that will be elaborate upon within this section relates to the behaviour of the foam under compression. This is a property of varying significance across each risk control option but, in general, the foam requires sufficient compressive strength with which to resist expected water pressures whilst at the same time being sufficiently elastic in order to absorb vibrations and sustain hydro-elastic effects.

In determining the foam compressive strength characteristics, two experiments were conducted on a foam specimen of 100 × 100 × 50 mm in size. In each case, the foam samples were placed within a compression-testing machine where they underwent 10% and 50% deformation, respectively. Figure 9 shows the tests for both deformations.

(**a**) (**b**)

Figure 9. Compression-cycle press/hold/release; (**a**) 10% deformation, (**b**) 50% deformation.

Figure 10 shows the results of this process, where the foam stress–strain curve is presented. Here, the foam displays linear elasticity under compressive pressure up to about 0.22 MPa (22 m water head), in which the foam cell walls compress and bend. Past this point, the foam cell walls begin to buckle, fracture, and yield, resulting in permanent deformation (plastic behaviour). This represents significant compressive strength and far exceeds expected water pressure heads, which are of the order of 10 m. Furthermore, though the degree of deformation that takes place within the elastic region is slight, <5%, this is more than enough to absorb any vibrations and hydro-elastic loads that may be expected.

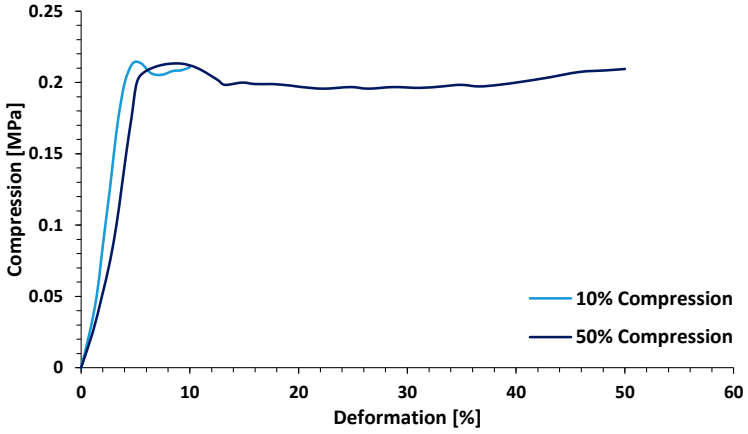

Figure 10. Foam stress–strain curve under compression.

3.3.4. Fire Performance

As polyurethane foam is an organic material, it is subject to thermal decomposition when exposed directly to fire or elevated temperatures. For this reason, a range of fire tests were conducted on the foam material to assess its fire performance and identify any potential risk sources. The results of this process were then used to establish suitable RCOs, such that any risk from the foam installation in relation to fire is suitably protected against.

As mentioned in previous sections, the areas targeted for foam application are enclosed void spaces, which are a category of space that pose negligible risk as a source of fire. Furthermore, introduction of foam material to the void works to displace oxygen from within the space, thus further reducing the likelihood of fire originating from any foam-protected void space. Consequently, foam installations do not pose any risk as a fire source or space of origin, but instead, the risk stems from the possibility of fire erupting in adjacent spaces. In such an event, it is possible that sufficient heat could be transferred into the foamed void, such as to give rise to foam decomposition, which could in turn result in gas overpressure within the void space. For this reason, the fire tests conducted on the foam material focused on establishing under what conditions foam thermal decomposition occurred, with specific attention given to the following parameters:

- Temperature;
- Exposure time;
- Magnitude of decomposition;
- Gas overpressure potential.

Two primary experiments were conducted in order to gain a greater understanding of the foam thermal decomposition behaviour. Within the first, differential thermal analysis (DTA) was conducted to determine the decomposition characteristics of the foam material and under which conditions this occurred. Here, loss in foam mass by virtue of thermal decomposition was measured with respect to temperature and exposure time using a thermogravimetric analyser and a sample of the foam material.

The results of this analysis are summarised within Table 3 below, where it can be observed that the foam sample is relatively stable up to temperatures within the range 180–200 °C, beyond which more extensive decomposition occurs. Below this temperature

range, only minor decomposition of 4% in foam mass was observed over three hours. Furthermore, limited sensitivity in the magnitude of decomposition with respect to time can be observed at temperatures below 200 °C, with an additional decrease in foam mass of only 3% recorded between 1 and 3 h of exposure time at 180 °C. It should also be noted that the results of this analysis are inherently conservative as all sides of the foam material were exposed to the temperature increments specified. However, in actuality, the degree of the foam body exposed to increased temperatures by virtue of fire would likely be localised in nature, thus leading to lower decomposition.

Table 3. Foam decomposition, temperature, and exposure time relationship.

Temp. (°C)	Residual Foam Weight after Time (% Original Weight)			
	0 h	1 h	2 h	3 h
140	100%	100%	100%	99%
160	100%	97%	96%	96%
180	100%	95%	93%	91%
200	100%	95%	89%	82%
220	100%	79%	67%	63%
240	100%	66%	64%	63%

Perhaps what is most significant about these findings is the indication that if the foamed void were equipped with suitable fire insulation, it could be ensured that decomposition temperatures were not realised. To investigate this, A-class fire insulation material from a well-known supplier was assessed in order to identify the specification that would be required to avoid foam decomposition. With the knowledge that the proposed foam technology undergoes thermal decomposition at temperatures above 160 °C, this can be considered the limiting temperature of the unexposed surface of the insulated bulkhead in determining the fire insulation requirements. Considering a maximum exposed surface temperature of 945 °C, as per IMO conditions for fire insulation testing, the results of this investigation are provided in Figure 11. Here, the temperature following 60 min at the unexposed foam/rockwool interface is plotted relative to insulation thickness. The findings indicate that a minimum insulation thickness of 60 mm is sufficient to avoid foam decomposition, making this a highly effective RCO.

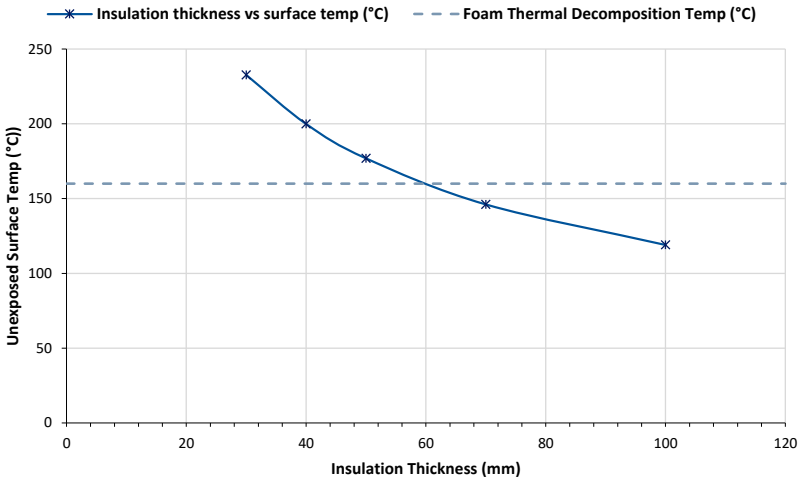

Figure 11. Insulation thickness relative to unexposed bulkhead surface temperature.

Despite the above indicating that fire insulation could be effectively utilised as an RCO to protect against foam decomposition, a secondary and highly novel experiment was also conducted, looking into foam decomposition and gas overpressure relative to temperature and time. The impetus for such an investigation was driven by a policy of

due diligence and rather conservative conditions were addressed in its undertaking. The experiment was conducted using a steel container of dimensions 500 × 150 × 150 mm, which was filled with foam material and equipped with pressure sensors located on either end of the apparatus. In addition, six thermocouples spaced equidistantly along the length of the box were installed to monitor the temperature throughout the experiment and at various depths within the foam body. See Figures 12 and 13 for details on the apparatus.

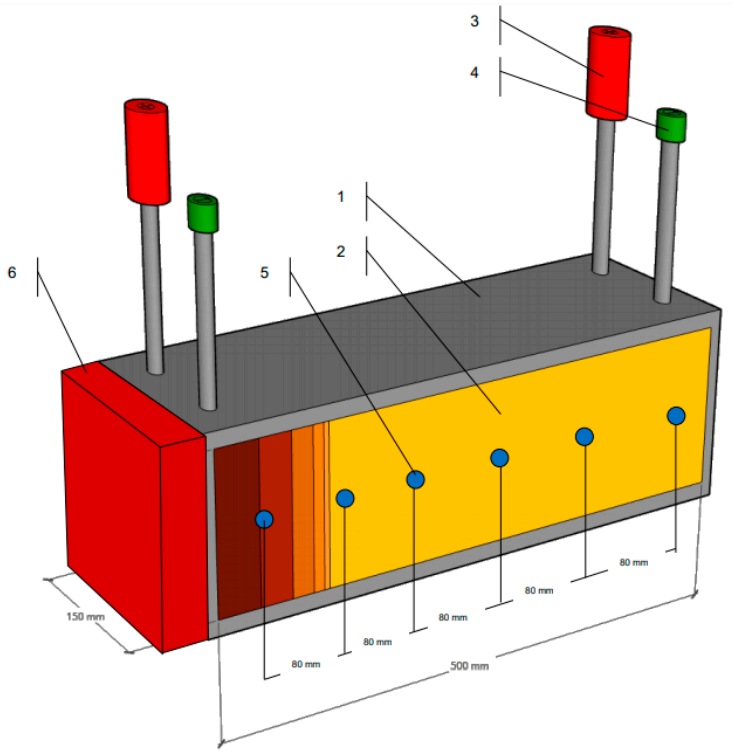

Figure 12. Apparatus schematic.

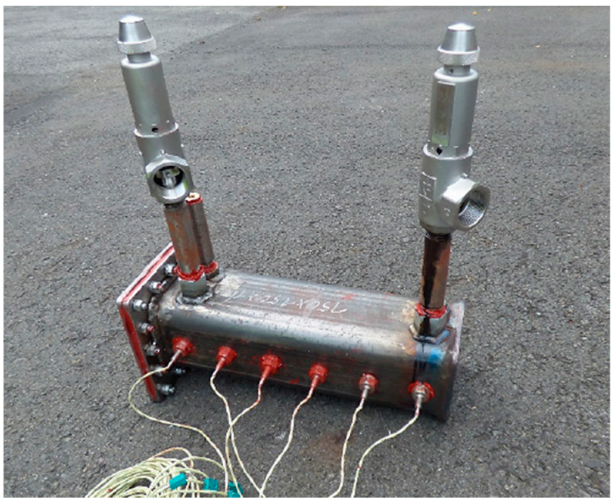

Figure 13. Apparatus as-built.

A contact heating plate was then applied to one end of the box and used to apply a constant temperature load of 300 °C for a period of 180 min. No insulation was applied at the foam/heating plate interface, thus making the test highly conservative as the foam was exposed to temperatures approximately double those expected with insulation in place. The results of the experiment are provided in Figures 14 and 15, shown below.

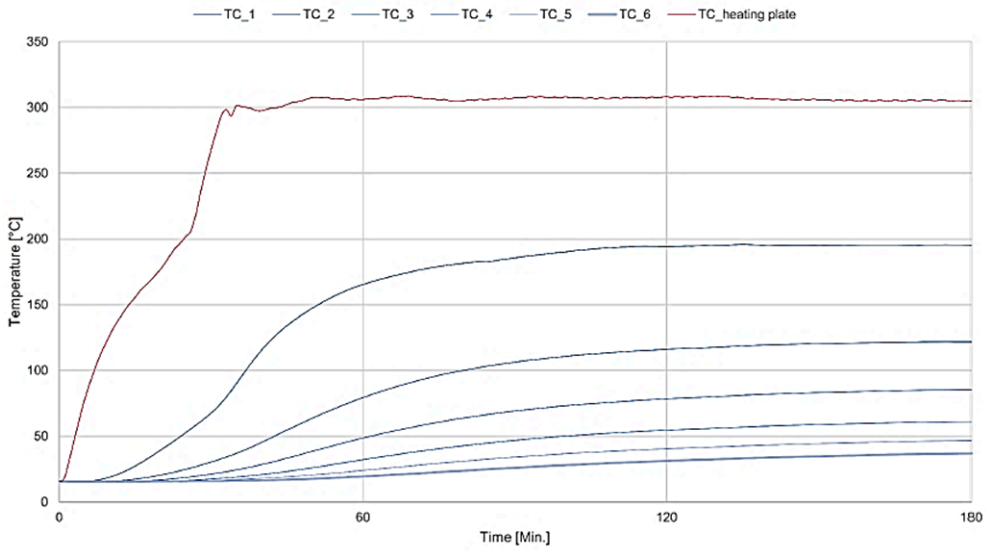

Figure 14. Temperature development for individual sensors.

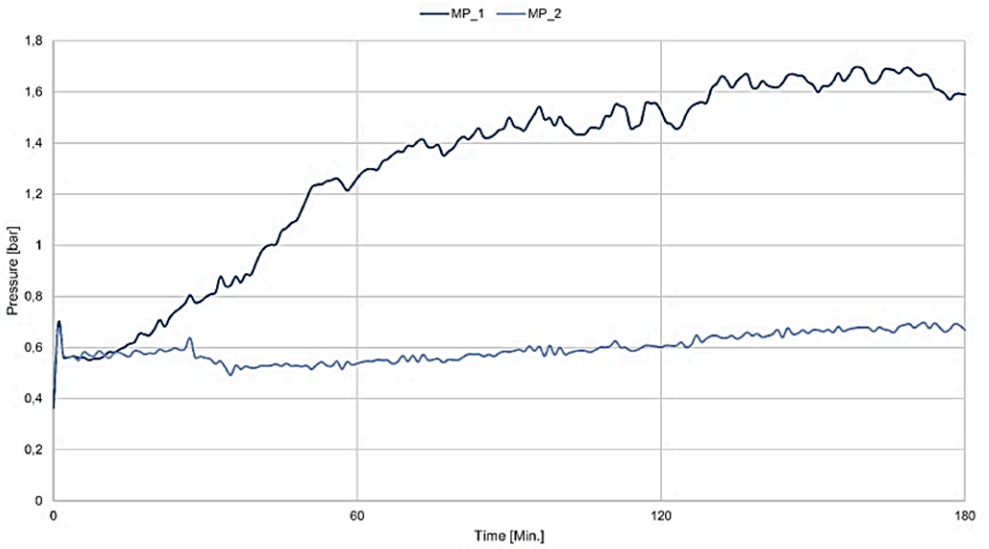

Figure 15. Development of gas pressure.

The results reveal that foam decomposition occurs only within the immediately affected area of the foam body, where temperatures exceed 160 °C. Otherwise, the spread of heat deeper into the foam body was found to be slow and minimal due to the insulating properties of the foam. In fact, at a distance of just 50 mm from the interface (TC_1), a temperature of only 165 °C was measured after 60 min and with a local gas pressure of 1.26 bar (0.126 MPa). This indicates that, even in the absence of fire insulation, the degree and rate of foam decomposition is minimal, and the resultant gas overpressure poses no risk to the void structural integrity.

4. Application on a Reference Passenger Ship

This section provides an overview of the methodology adopted and supporting calculations in the assessment of the effectiveness of the proposed AREST P1 and A2 systems as a means of passive and active damage stability protection through internal reconfiguration. The application of the AREST system was studied on the reference cruise ship C1, with the main particulars reported in Table 4 and the hull geometry shown in Figure 16.

Table 4. General particulars for cruise ship C1.

Quantity	Value	Unit
Length overall	317.2	m
Length between perpendiculars	293.7	m
Subdivision length	316.2	m
Breadth moulded	36.8	m
Draught, subdivision	8.6	m
Draught, design	7.3	m
No. passengers	3148	persons
No. crew	1252	persons

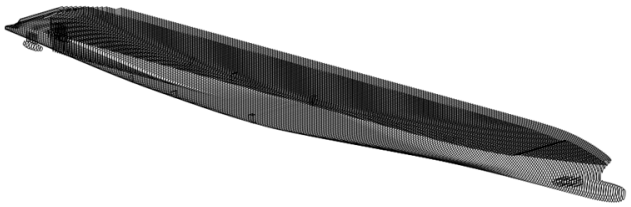

Figure 16. Hull geometry for cruise ship C1 used for stability calculations.

The following process was developed to identify the location of passive and active countermeasures to increase the ship's safety, using both static and dynamic calculations. The procedure can be summarised in the following steps:

1. Static damage stability assessment for the ship as it is according to SOLAS [7] and determination of GM margins for the ship as it is.
2. Reconfiguration of the internal layout with AREST P1 permanent foam installation.
3. Determination of GM margins for the reconfigured ship.
4. Dynamic assessment of the ship with AREST P1 configuration.
5. Identification of critical openings to place AREST A2 barriers and evaluation of new GM margins with both AREST P1 and AREST A2 solutions.

The present study addresses the specific case of collision damages only; however, the process can be applied for other damage types as side or bottom groundings.

4.1. Static Damage Stability Assessment for the Original Ship

The vessel was first subjected to damage stability assessment (using the process described in Section 2 for collisions) under her present GM limit curve conditions, which were proven to be optimal with the vessel, achieving an attained index of 0.830 with a required index of 0.829, as shown in Table 5.

Table 5. Attained index calculations for cruise ship C1 with original layout.

Condition	T (m)	GM (m)	A_k	w_k	$A_k w_k$
Light service	8.00	2.57	0.846	0.2	0.1692
Partial subdivision	8.36	2.49	0.829	0.4	0.3315
Deepest subdivision	8.60	2.64	0.822	0.4	0.3289
		Attained Index			0.830
		Required Index			0.829

The vessel static risk profile is shown in Figure 17. This demonstrates vulnerability around the fore and aft shoulders, which is typical of cruise vessels. This risk can be attributed to a combination of both lack of reserve buoyancy and residual GM, in addition to having an insufficient range to the immersion of unprotected openings.

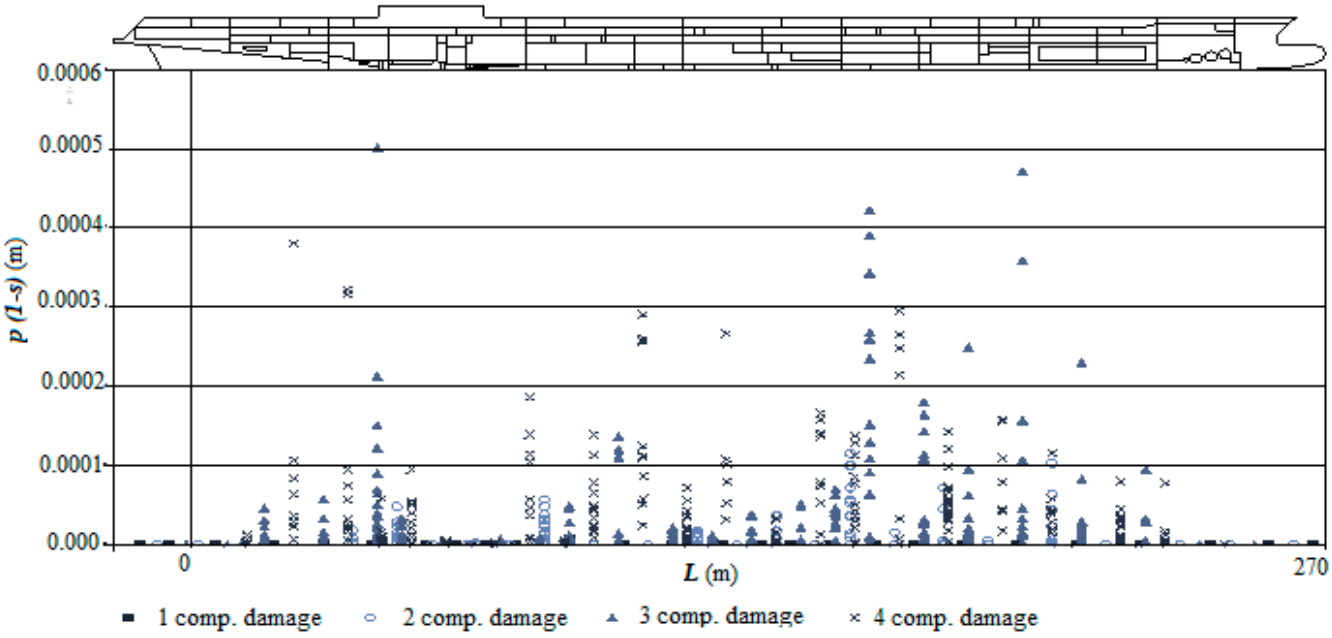

Figure 17. Static risk profile for cruise ship C1 with original layout.

The stability booklet for vessel C1 has in total eight relevant loading conditions. Observation of the vessel GM limit curve highlights that GM margins in some 40% of cases lie below 10 cm. By predicting an annual increase in vessel lightweight KG by 2 cm (in line with previous growth trends), additional GM margins of approximately 35 cm for all loading cases are required in order to remain compliant in 20-years' time. This was estimated using a constant lightweight value but having altered the vertical centre of gravity by 40 cm for each statutory loading condition. Table 6 summarises the GM margins evaluated for the original cruise ship layout.

Table 6. Loading conditions and GM margins for cruise ship C1 with the original layout.

ID	Condition	T (m)	GM (m)	GM Req. (m)	GM Margin (m)	$\Delta GM_{20yr.}$ (m)
LC1	100% Cons. Max. Draught	8.601	2.83	2.65	0.18	0.337
LC2	75% Bunkers and stores	8.370	2.64	2.50	0.14	0.339
LC3	50% Bunkers and stores	8.259	2.56	2.51	0.05	0.360
LC4	25% Bunkers and stores	8.195	2.56	2.53	0.03	0.358
LC5	Arrival condition	8.160	2.55	2.54	0.01	0.355
LC6	Ballast departure condition	8.565	2.94	2.62	0.32	0.337
LC7	Ballast arrival condition	8.123	2.66	2.55	0.11	0.356
LC8	Docking condition	8.304	2.68	2.51	0.17	0.347

4.2. Internal Layout Reconfiguration with AREST P1 System

The following provides a summary of all proposed permanent foam installation locations as shown in Figure 18, determined according to the static risk profile of Figure 17. In addition, a breakdown of all foam volumes and installation weights is provided within Table 7. The locations of the foam installations were focused within areas found to possess the highest flooding risks. The foam was also located predominantly around decks 1 and 2, which lie within the region of the damaged waterline and above, thus providing both buoyancy and stability at equilibrium and as the vessel is heeled from this position.

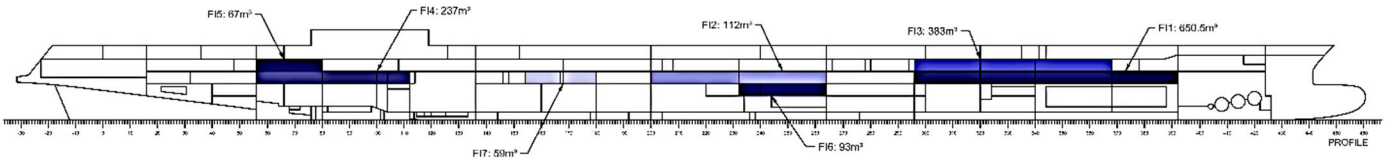

Figure 18. AREST P1 permanent foam installations for cruise ship C1.

Table 7. AREST P1 foam installation volumes and weights.

ID	Foam Volume (m^3)	Additional Weight (ton)
F1	651	8.131
F2	112	1.400
F3	383	4.788
F4	237	2.963
F5	67	0.839
F6	93	1.163
F7	59	0.738
TOTAL	1601.5	20.019

4.3. Static Assessment and GM Margins for the Reconfigured Vessel (AREST P1)

Following remodelling of the vessel internal geometry with permanent foam modifications, the vessel damage stability performance was reassessed in order to ascertain the new GM limiting values. This process is alternative to evaluate a new *A* index according to the old limiting GM values and results in the determination of new margins for the vessel loading conditions. Table 8 reports the updated results of static stability assessment. In such a case, there is no need for a re-evaluation of the static risk profile. In fact, being the strategy oriented to find the new limiting GM, the resulting s-factors are the minimum ones granting to achieve the compliance with the required index criteria. Thus a new static risk profile will highlight vulnerability in the same areas of the vessel in the original configuration.

Table 8. Attained index calculations for cruise ship C1 with AREST P1 reconfiguration.

Condition	T (m)	GM (m)	A_k	w_k	$A_k w_k$
Light service	8.00	2.40	0.840	0.2	0.1680
Partial subdivision	8.36	2.28	0.822	0.4	0.3286
Deepest subdivision	8.60	2.49	0.831	0.4	0.3323
		Attained Index			0.829
		Required Index			0.829

With the proposed modifications, GM margins increased between 16 and 21 cm, with the resultant margins now ranging between 20 and 48 cm (see Table 9). Considering the projected growth in vessel lightweight KG of 2 cm/year, 50% of statutory loading conditions can now survive this growth without jeopardising compliance. Therefore, the aforementioned design vulnerability could turn into a very effective passive flooding protection system with permanent foam installation in high-risk void spaces.

Table 9. Loading conditions and GM margins for cruise ship C1 with AREST P1 reconfiguration.

		Existing		AREST P1	
ID	**GM (m)**	**GM Req. (m)**	**GM Margin (m)**	**GM Req. (m)**	**GM Margin (m)**
LC1	2.83	2.65	0.18	2.49	034
LC2	2.64	2.50	0.14	2.29	0.35
LC3	2.56	2.51	0.05	2.31	0.25
LC4	2.56	2.53	0.03	2.34	0.23
LC5	2.55	2.54	0.01	2.35	0.20
LC6	2.94	2.62	0.32	2.46	0.48
LC7	2.66	2.55	0.11	2.36	0.30
LC8	2.68	2.51	0.17	2.30	0.38

4.4. Dynamic Assessment of the Ship with AREST P1 Configuration

Static assessment techniques cannot capture a number of key characteristics of the flooding process. This includes, but is not limited to, the identification and distinction of the aforementioned loss modalities (transient or progressive flooding capsize), the impact of wave induced effects and the ability to measure time to capsize. Time domain simulations allow vessel survivability to be viewed from different, more physics-based and more detailed perspectives, enabling to identify aspects ignored within a conventional static assessment. Therefore, it is useful to dynamically assess damage stability of the initial and reconfigured ship to check whether the static improvements also maintain when considering waves.

On the basis of the aforementioned considerations, the vessel was assessed at a single loading condition corresponding to the deepest subdivision draft and associated limiting GM. The simulations were performed in irregular waves (JONSWAP spectrum) with a fixed significant wave height of Hs = 4 m, representing the upper limit of the SOLAS wave distribution (stress testing of the vessel). In total, 1500 collision damage simulations were conducted with an exposure time of 30 min, with 10 repetitions per case.

The results produced for the vessel in the original configuration have highlighted 22 capsize cases (3 progressive flooding cases/19 transient capsize cases), which translates to a survivability index of 0.987, applying Equation (8). The results of simulations with AREST P1 demonstrated a reduction in capsize cases from 22 to 15; all the cases are transient capsizes. Figure 19 shows the location of the residual loss scenarios for the two configurations; the differences in the time to capsize for the same damage cases are reported in Figure 20. Based on the updated results, the vessel survivability index for 30 min of exposure time increased from 0.987 to 0.992.

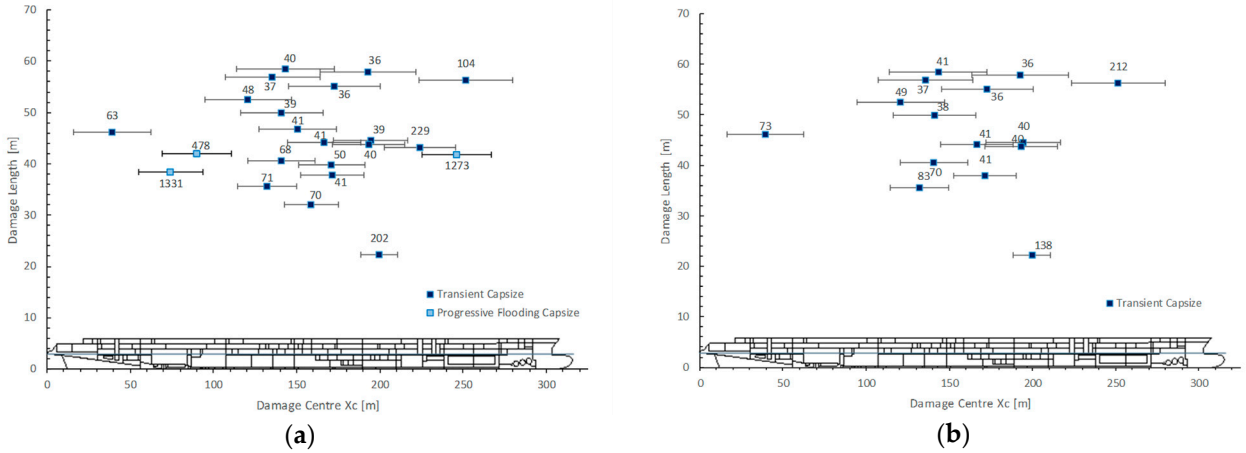

Figure 19. Residual loss scenarios. (**a**) Original layout, (**b**) AREST P1 reconfiguration.

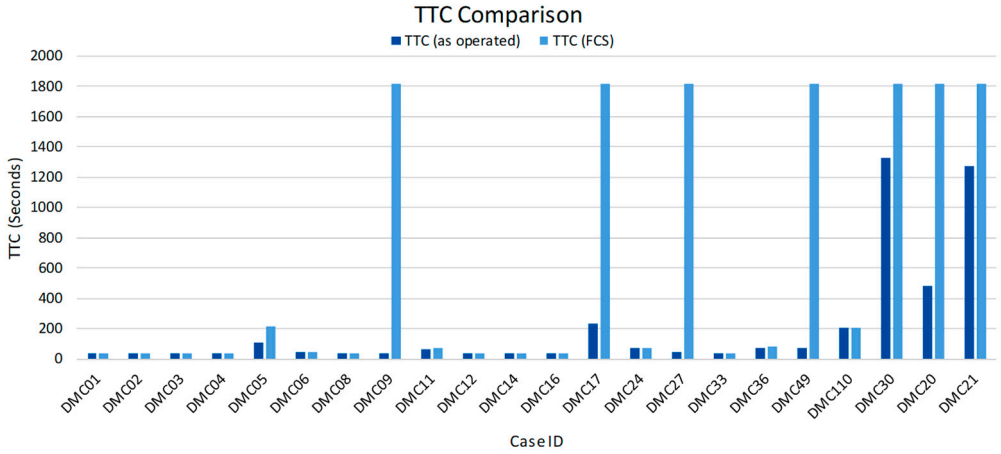

Figure 20. Time to capsize comparison on residual loss scenarios with and without AREST P1.

The results were scrutinised further in order to identify vulnerable design features within the vessel design and, more specifically, the sources of this vulnerability to transient cases. Through doing so, inadequate cross-flooding/equalization within machinery and accommodation spaces was identified as a primary causal factor. The means of transverse communication within these spaces are predominantly manhole-sized openings and narrow corridors. An overview of the primary sources of cross-flooding restriction is provided in Figure 21, where they are marked in blue.

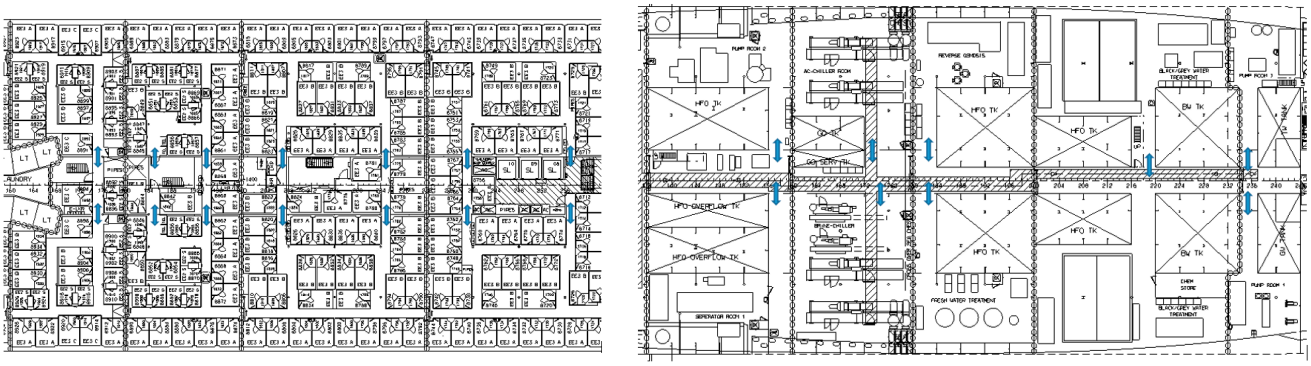

(**a**) (**b**)

Figure 21. Cross-flooding restriction sources. (**a**) Deck 1, (**b**) tank top deck.

4.5. AREST A2 System Implementation

The AREST A2 system is a protection aimed at limiting progressive flooding. However, the provided example highlights that the AREST P1 system is sufficient to avoid progressive flooding occurrences within the simulated collision cases. Nonetheless, this system can also be used to protect critical openings and provide further increased GM margins.

This assessment was conducted with a specific focus on critical openings, which are proposed to be protected by the AREST A2 system. As GM margins are determined on the basis of statutory requirements, this assessment was conducted using hydrostatic damage stability calculations. Unfortunately, this form of damage stability assessment cannot model the effects of progressive flooding in the physical sense and instead the potential for progressive flooding is captured through the modelling of unprotected openings. These have the effect of truncating the damaged GZ curve, which in turn reduces the *Range* and GZ_{max} values that may be used in the determination of the s-factor. As such, the modelling of such an opening accounts for the risk of progressive flooding, albeit in an indirect sense. Given this, the approach adopted was to calculate the degree in which the influence of each unprotected opening affects the potential A-Index contribution belonging to each damage

case and verifying this with the simulation results. By doing so, openings can be ranked in order of criticality measured by lost index. This, in turn, can be used to inform which opening deployable barriers would best protect from a risk reduction perspective.

A set of 15 openings was found to be critical. Having targeted the openings, the vessel damage stability performance was re-evaluated, with these openings assumed watertight and the existing passive foam solution in place. The results show that in protecting just the four openings specified, the vessel GM margins can be increased by an additional 10 cm across the entire draft range. This then yields a net benefit, in respect to both solutions, of 30–56 cm, as summarised within Table 10. The same can be reported in form of the percentage of GM, highlighting how the AREST systems increase the GM margins from 5 to 11% of GM compared to the original design.

Table 10. Loading conditions and GM margins for cruise ship C1 with AREST systems.

	Existing			AREST P1		AREST P1+A2	
ID	**GM (m)**	**GM Req. (m)**	**GM Margin (m)**	**GM Req. (m)**	**GM Margin (m)**	**GM Req. (m)**	**GM Margin (m)**
LC1	2.83	2.65	0.18	2.49	0.34 (+5.65% GM)	2.40	0.43 (+8.83% GM)
LC2	2.64	2.50	0.14	2.29	0.35 (+7.95% GM)	2.21	0.43 (+10.98% GM)
LC3	2.56	2.51	0.05	2.31	0.25 (+7.81% GM)	2.23	0.33 (+10.94% GM)
LC4	2.56	2.53	0.03	2.34	0.23 (+7.81%GM)	2.24	0.32 (+11.33% GM)
LC5	2.55	2.54	0.01	2.35	0.20 (+7.45% GM)	2.26	0.30 (+11.37% GM)
LC6	2.94	2.62	0.32	2.46	0.48 (+5.44% GM)	2.38	0.57 (+8.51% GM)
LC7	2.66	2.55	0.11	2.36	0.30 (+7.15% GM)	2.27	0.39 (+10.53% GM)
LC8	2.68	2.51	0.17	2.30	0.38 (+7.84% GM)	2.22	0.46 (+10.82% GM)

5. Conclusions

The present work provides an overview of the possible advantages in terms of safety given by the installation of active and passive risk control options against flooding. Two solutions based on the application of high expansion foam were described, being part of the AREST system, a technology developed at the University of Strathclyde in collaboration with worldwide industrial partners. The focus on both passive (AREST P1) and active (AREST A2) countermeasures also concerns the mechanical properties of the foam, necessary to grant adequate permeability, adhesion, and cohesion characteristics to be efficiently employed onboard ships.

The application on a reference cruise ship highlights the potential benefits in terms of increased stability margins provided by the system. These advantages can be evaluated by means of conventional static calculations, easily implementable by naval architects, providing results of clear interpretation by designers and cruise ship operators. However, it was demonstrated that, by adopting more advanced and higher fidelity time domain simulations in waves, more insight in the flooding process can be achieved, detecting design weaknesses in the ship's internal layout invisible to conventional calculations.

The proposed approach to investigate the application of the AREST risk control option onboard passenger ships need to be further refined, studying a better synergy between static and dynamic analyses, which, in the present work, remains fully dissociated. The development of an integrated static–dynamic process will increase the advantages of using a dynamic damaged ship simulation in the ship design. Furthermore, the applications of deployable barriers, as in the case of the AREST A2 system, require a proper study of ship evacuation, in such a way to prevent the interruption of principal escape routes crucial for ship evacuation.

Nonetheless, the present work clearly indicates that the application of modern technologies employing foam materials, as the AREST system, is the right way to further increase ship safety against flooding, without employing drastic changes in the internal layout of the vessel, thus decreasing the earning capacity of the ship.

Author Contributions: Conceptualization, D.V., F.M. and D.P.; methodology, D.V., F.M. and D.P.; formal analysis, D.P., G.A., P.A., A.J. and F.M.; investigation, D.P., G.A., P.A., A.J. and F.M.; data curation, D.P. and F.M.; writing—original draft preparation, F.M., D.V. and D.P.; writing—review and editing, D.V., D.P. and F.M.; visualization, D.P. and F.M.; supervision, D.V. All authors have read and agreed to the published version of the manuscript.

Funding: This research was funded by the Scottish Government, grant number SA1256, Royal Caribbean Cruises, MINOVA, and Maritime Safety Innovations, Ltd. (Glasgow, UK).

Informed Consent Statement: Not applicable.

Data Availability Statement: Not applicable.

Conflicts of Interest: The authors declare no conflict of interest.

References

1. Vanem, E.; Rusas, S.; Skjong, R.; Olufsen, O. Collision damage stability of passenger ships: Holistic and risk-based approach. *Int. Shipbuild. Prog.* **2007**, *54*, 323–337.
2. Vassalos, D.; Guarin, L. Designing for damage stability and survivability—Contemporary developments and implementation. *Ship Sci. Technol.* **2009**, *1*, 59–71.
3. Spanos, D.; Papanikolaou, A. Considerations on the survivability assessment of damaged ships. In Proceedings of the 12th International Ship Stability Workshop (ISSW2011), Washington, DC, USA, 12–15 June 2011.
4. Clarksons Shipping. Available online: https://www.clarksons.com (accessed on 12 December 2021).
5. Vassalos, D. Damage survivability of cruise ships—Evidence and conjecture. *Ocean Eng.* **2016**, *121*, 89–97. [CrossRef]
6. IMO. *International Convention for the Safety of Life at Sea (SOLAS)*; Consolidated Edition as of 2009; IMO: London, UK, 2009.
7. IMO. *International Convention for the Safety of Life at Sea (SOLAS)*; Consolidated Edition as of 2020; IMO: London, UK, 2020.
8. Vassalos, D.; Papanikolaou, A. A holistic view of Design for Safety. In Proceedings of the 7th International Maritime Safety Conference on Design for Safety, Kobe, Japan, 16–21 September 2018.
9. Woisin, G. Design against collisions. In Proceedings of the International Symposium on Advances in Ship Technology, Trondheim, Norway, 2 June 1979.
10. Storheim, M.; Amdahl, J. Design of offshore structures against accidental ship collisions. *Mar. Struct.* **2014**, *37*, 135–172. [CrossRef]
11. King, T.; Van Welter, C.; Svensen, T.E. Stability barrier management for large passenger ships. *Ocean Eng.* **2016**, *125*, 342–348. [CrossRef]
12. Vassalos, D.; Paterson, D. Towards unsinkable ships. *Ocean Eng.* **2020**, *232*, 109096. [CrossRef]
13. Paterson, D. Reconfiguring the Ship Environment for Damage Stability Enhancement. Ph.D. Thesis, University of Strathclyde, Glasgow, UK, 2020.
14. Van't Veer, R.; De Kat, J.; Cojeen, P. Large Passenger Ship Safety: Time-to-Flood Simulations. *Mar. Technol. SNAME News* **2004**, *41*, 82–88. [CrossRef]
15. Vassalos, D. The role of damaged ship dynamics in addressing the risk of flooding. *Ship Offshore Struct.* **2020**, *17*, 279–303. [CrossRef]
16. Vassalos, D.; Patterson, D. Reconfiguring passenger ship internal environment for damage stability enhancement. *J. Mar. Sci. Eng.* **2020**, *8*, 693. [CrossRef]
17. Vassalos, D.; Paterson, D.; Boulougouris, E.; Mauro, F. Life-cycle stability management for passenger ships. In Proceedings of the International Offshore and Polar Engineering Conference, Rhodes, Greece, 20–25 June 2021; pp. 2786–2793.
18. Naar, H.; Kujala, P.; Simonsen, B.C.; Ludolphy, H. Comparison of the crashworthiness of various bottom and side structures. *Mar. Struct.* **2002**, *15*, 443–460. [CrossRef]
19. Kang, H.J.; Kim, I.; Choi, J.; Lee, G.J.; Park, B.J. A concept study for the buoyancy support system based on the fixed fire-fighting system for damaged ships. *Ocean. Eng.* **2018**, *155*, 361–370. [CrossRef]
20. Jalonen, R.; Ruponen, P.; Weryk, M.; Naar, H.; Vaher, S. A study on leakage and collapse of non-watertight ship doors under floodwater pressure. *Mar. Struct.* **2017**, *51*, 188–201. [CrossRef]
21. Van't Veer, R.; Peters, W.; Rimpelä, A.-L.; De Kat, J. Exploring the Influence of Different Arrangements of Semi-Watertight Spaces on Survivability of a Damaged Large Passenger Ship. In Proceedings of the 7th International Ship Stability Workshop, Shanghai, China, 2–3 November 2004.
22. Papanikolaou, A.; Hamann, R.; Lee, B.S.; Mains, C.; Olufsen, O.; Tvedt, E.; Vassalos, D.; Zaraphonitis, G. GOALDS—Goal-based damage stability of passenger ships. In Proceedings of the SNAME Maritime Convention 2013 (SMC 2013), Bellevue, WA, USA, 8 November 2013.
23. Atzampos, G. A Holistic Approach to Damage Survivability Assessment of Large Passenger Ships. Ph.D. Thesis, University of Strathclyde, Glasgow, UK, 2019.
24. Lützen, M. Ship Collision Damage. Ph.D. Thesis, Technical University of Denmark, Lyngby, Denmark, 2001.
25. Bulian, G.; Cardinale, M.; Dafermos, G.; Lindroth, D.; Ruponen, P.; Zaraphonitis, G. Probabilistic assessment of damaged survivability of passenger ships in case of grounding or contact. *Ocean Eng.* **2020**, *218*, 107396. [CrossRef]

26. Bulian, G.; Lindroth, D.; Ruponen, P.; Zaraphonitis, G. Probabilistic assessment of damaged ship survivability in case of grounding: Development and testing of a direct non-zonal approach. *Ocean Eng.* **2016**, *120*, 331–338. [CrossRef]
27. Zang, M.; Montewka, J.; Manderbacka, T.; Kujala, P.; Hirdaris, S. A Big Data Analytics Method for the Evaluation of Ship-Ship Collision Risk reflecting Hydromeeorological Conditions. *Reliab. Eng. Syst. Saf.* **2021**, *213*, 107674. [CrossRef]
28. Zang, M.; Conti, F.; Le Sourne, H.; Vassalos, D.; Kujala, P.; Lindroth, D.; Hirdaris, S. A method for the direct assessment of ship collision damage and flooding risk in real conditions. *Ocean Eng.* **2021**, *237*, 109605. [CrossRef]
29. Conti, F.; Le Sourne, H.; Vassalos, D.; Kujala, P.; Lindroth, D.; Kim, S.J.; Hirdaris, S. A comparative method for scaling SOLAS collision damage distributions based on a ship crashworthiness-application to probabilistic damage stability analysis of a passenger ship. *Ship Offshore Struct.* 2021, *in press*. [CrossRef]
30. Bulian, G.; Cardinale, M.; Dafermos, G.; Eliopoulou, E.; Francescutto, A.; Hamann, R.; Lindroth, D.; Luhmann, H.; Ruponen, P.; Zaraphonitis, G. Considering collision, bottom grounding and side grounding/contact in a common non-zonal framework. In Proceedings of the 17th International Ship Stability Workshop, Helsinki, Finland, 10–12 June 2019; pp. 245–257.
31. Vassalos, D.; Mujeeb-Ahmed, M.P.; Paterson, D.; Mauro, F.; Conti, F. Probabilistic Damage Stability for Passenger Ships—The p-Factor Illusion and Reality. *J. Mar. Sci. Eng.* **2022**, *10*, 348. [CrossRef]
32. Pawlowski, M. *Subdivision and Damaged Stability of Ships*; Euro-MTEC Book Series; Fundacja Promocji Przemyslu: Gdansk, Poland, 2004.
33. Mauro, F.; Vassalos, D. The influence of damage breach sampling process on the direct assessment of ship survivability. *Ocean Eng.* **2022**, *250*, 111008. [CrossRef]
34. Jasionowski, A. An Integrated Approach to Damage Ship Survivability Assessment. Ph.D. Thesis, University of Strathclyde, Glasgow, UK, 2001.
35. Papanikolaou, A.; Zaraphonitis, G.; Boulougouris, E.; Eliopoulou, E. Investigation into the capsizing of damaged Ro-ro passenger ship in waves. In Proceedings of the STAB Conference, Lounceston, Australia, 7–12 February 2000.
36. Paterson, D.; Atzampos, G.; Vassalos, D.; Boulougouris, E. Impact of wave statistics on ship survivability. In Proceedings of the 16th International Ship Stability Workshop, Belgrade, Serbia, 5–7 June 2017.
37. D'Amore, G.K.O.; Marinò, A.; Kaspar, J. Numerical modelling of fire resistance test as a tool to design lightweight fire doors: A preliminary study. *J. Mar. Sci. Eng.* **2020**, *8*, 520. [CrossRef]
38. D'Amore, G.K.O.; Mauro, F.; Marinò, A.; Caniato, M.; Kaspar, J. Towards the use of novel materials in shipbuilding: Assessing thermal performances of fire-doors by self-consistent numerical modelling. *Appl. Sci.* **2020**, *10*, 5736. [CrossRef]
39. Caniato, M.; D'Amore, G.K.O.; Kaspar, J.; Gasparella, A. Sound absorption performance of sustainable foam materials: Application of analytical and numerical tools for the optimization of forecasting models. *Appl. Acoust.* **2020**, *161*, 107166. [CrossRef]